10.6

SHORT-TERM FORECASTING OF AIRPORT SURFACE VISIBILITY USING RADAR AND ASOS

Michael Dixon, Roy M. Rasmussen, and Scott Landolt
National Center for Atmospheric Research*, Boulder, Colorado

Abstract: Surface visibility is important for airport operations, since it affects the VFR/IFR status and category. This study demonstrates a method of making short-term visibility forecasts using an approach similar to that employed in the Weather Support to Deicing Decision Making (WSDDM) snow rate forecast. The ASOS installations at each major airport include sensors which measure visibility. This study uses those visibility measurements, along with radar observations and other ASOS data, to determine a relationship between radar reflectivity and visibility during snow conditions. This relationship is used together with an extrapolation forecast of radar reflectivity to determine forecast visibility during snow conditions out to one hour. The paper will present an evaluation of the technique at airports in the New York area.*

1 INTRODUCTION

For the past 6 years the FAA-sponsored Weather Support to Deicing Decision Making (WSDDM) system has included a component which produces a short-term forecast of snowfall rate at the surface using gauge-calibrated radar.

The WSDDM snowfall-forecasting algorithm has demonstrated that it is possible to use radar reflectivity and radial velocity data to track and forecast the motion of snow squalls and snow bands. This motion information, combined with surface wind data and the estimated fall speed of snow particles, allows the WSDDM algorithms to forecast the precipitation rate of snow at the ground. Gauges at ground sites accurately record the actual snow rate. This gauge-measured data provides the ground truth from which the relationship between radar reflectivity and snow rate is computed.

Surface visibility is important for airport operations, since it affects the VFR/IFR status and category. This study considers the feasibility of making short-term visibility forecasts using an approach similar to that employed in the WSDDM snow rate forecast. The ASOS installations at each major airport include sensors which measure visibility. This study uses those visibility measurements, along with radar observations and other ASOS data, to investigate the relationship between radar reflectivity and visibility and to determine whether it is feasible to base a short-term visibility forecast on these observations.

We will show that in order to make an accurate forecast we need to understand how snow particles move from where they are detected by radar to where they arrive at the ground and impact visibility.

Specifically, the following must be determined:

- the motion of the radar echo;
- the vertical wind profile from the radar beam height to the surface;
- the time taken for the particles to fall from the radar beam height to the surface.

We will also show that it is possible to compute visibility from radar reflectivity provided the specified calibration procedure is followed.

2 Observations and data sets

2.1 ASOS visibility measurements

Each ASOS installation includes one or more visibility sensors. In multiple-sensor installations the sensors are located at different points on the airport which allows assessment of the spatial variability of the visibility values.

ASOS uses a Belfort forward-scattering sensor to measure visibility (Nadolski and Gifford, 1995). The visibility is expressed in terms of Extinction Coefficient (E), with units of km^{-1}. E is a measure of the spatial rate of diminution or extinction of transmitted visible light (Huschke, 1959).

Visibility is inversely related to E. In the ASOS system, the visibility is computed from E using different formulae for day and night conditions (Nadolski and Gifford, 1995).

* Corresponding author address: Michael Dixon, RAP, NCAR, POBox 3000, Boulder, CO, 80307-3000, USA. Email: dixon@ucar.edu.

Day: $V = 3.0 / E$ (1)

Night: $0.00336 = e^{(-EM \times V)} / V$ (2)

The night equation assumes that the variables are expressed in statute miles rather than km. EM is used instead of E, where is EM expressed in units of mi^{-1}.

Table 1 shows examples of visibility computed for various E values for day and night operations.

E (km^{-1})	Day vis. (miles)	Night vis. (miles)	E (km^{-1})	Day vis. (miles)	Night vis. (miles)
0.10	18.64	17.58	1.50	1.24	2.06
0.15	12.43	12.98	2.00	0.93	1.62
0.20	9.32	10.42	2.50	0.75	1.34
0.25	7.46	8.76	3.50	0.53	1.01
0.30	6.21	7.60	4.00	0.47	0.90
0.35	5.33	6.73	4.00	0.47	0.90
0.40	4.66	6.05	5.00	0.37	0.75
0.50	3.73	5.06	6.00	0.31	0.64
0.60	3.11	4.37	7.00	0.27	0.56
0.70	2.66	3.86	8.00	0.23	0.50
0.80	2.33	3.46	9.00	0.21	0.45
1.00	1.86	2.88	10.00	0.19	0.41

Table 1: ASOS-derived visibility for various values of E

The day/night differences result from the fact that the human eye perceives objects during the day differently from light sources at night. Therefore effective visibility differs between day and night for the same E value. In this study we only consider E, thereby removing the complexity of different E-V relationships between day and night.

The E values measured by an ASOS station are averaged over a 1-minute period for smoothing. After visibility has been calculated from the E value, it is further averaged over a 10-minute period using an harmonic mean:

$$V_{Mean} = n/(1/V_1 + 1/V_2 + ... 1/V_n). \quad (3)$$

2.2 Other ASOS measurements

In addition to visibility, the ASOS stations measure a number of other variables. In this study we make use of wind speed and direction for determining the vertical wind profile. Follow-on work would probably incorporate the use of temperature and LEDWI precipitation category to discriminate between rain and snow.

2.3 Radar observations

Weather radar coverage of much of the continental United States is provided by the 150 or so 10-cm NEXRAD WSR88D radars run by the NWS. The data from these radars is made available via the NWS NOAA-port system as tertiary products in the NIDS format. These products are in the form of 2-D gridded data.

More recently the data has become available from selected sites in greater detail on a beam-by-beam basis, known as level-2 data. Such data would be probably improve the accuracy of this type of work but is not essential.

At major airports the WSR88D coverage is augmented by the 5-cm TDWR radars, which provide data at higher resolution and sensitivity.

Weather radars typically operate in a surveillance mode in which successive 360-degree revolutions are completed at a constant elevation angle (antenna angle above the horizon). Each constant-angle sweep is known as a Plan Position Indicator (PPI) product. Such measurements form a cone centered on the radar and elevated above the horizontal. PPIs start at a low elevation angle (typically 0.2 to 0.5 degrees) with increasing elevation angles for subsequent PPIs.

Since the raw radar data lies on a complicated 3-D conical coordinate system, the data was remapped onto a simpler Cartesian grid before being used in this study.

2.4 Data sets used in the study

The following data sets were obtained for use in this study:

(a) 1-minute ASOS data from La Guardia (LGA), Kennedy (JFK) and Newark (EWR) airports for the period 2002/01/31 through 2002/04/30 2002. Since there are multiple visibility sensors at each airport, the mean from the sensors was computed to represent the value for that airport.

(b) NIDS radar data from the OKX (Long Island) WSR88D radar for the period 2002/01/31 through 2002/04/30.

3 Theoretical aspects of the forecast

3.1 Advection-based nowcasting

'Nowcasting' refers to the technique of making short term forecasts by interpreting and extrapolating the latest observations. Nowcasting in the context of this study concentrates on how things *move* rather than how they *evolve*. This differs from model-based work which aims to forecast how systems evolve as well as how they move.

Advection is the technical term for the movement of elements within a weather system. Here we are aiming to make an advection-based forecast. It is therefore not surprising that much of the work concentrates on determining how the precipitation particles move from where they are detected by radar to where they arrive at the ground and affect the surface visibility.

3.2 Precipitation particle trajectories from radar to gauge

Since we wish to use the radar to predict the arrival of precipitation at the gauge, we need to consider the nature of the trajectory of the precipitation particles from the location at which the radar detects them to the point at which they are measured on the surface.

The beam from a weather radar radiates power to a *sample volume* some distance above the surface. The radar receiver processes the signal returned from that volume and interprets it as reflectivity (Z, power) and radial velocity (VR, velocity to/from the radar site).

Z represents the power returned from the contents of the sample volume - the higher the returned power the more 'severe' the weather in the beam. For display purposes Z is normally expressed in dBZ, where $dBZ=10\log_{10}(Z)$. VR is an estimate of how fast particles are moving towards or away from the radar, and is measured in m/s.

Figure 1 shows how a radar detects a weather echo aloft, and what the trajectory of the precipitation particles from the sample volume to the surface gauge might be. The sample volume is shown shaded. We use the motion of the radar echo to infer the wind vector at the height of the sample volume. In the situation depicted the surface wind and the movement of the radar echo aloft are the same, and there is no vertical wind shear. The particles theoretically will fall following a straight trajectory from the sample volume to the gauge. The source for the particles which arrive at the gauge is some distance ***upwind*** of the gauge, the distance being dependent on height of the sample volume and the ratio of the fall speed to the advection speed.

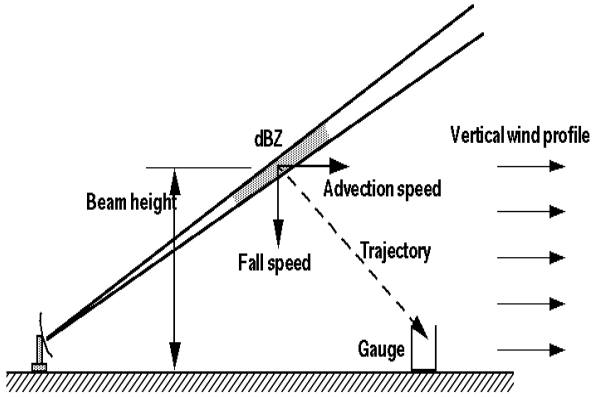

Figure 1: Particle trajectory for wind profile with no shear

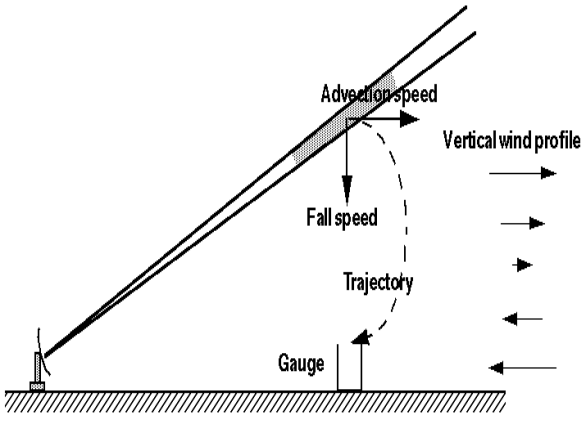

Figure 2: Particle trajectory for wind profile with shear

Figure 2 shows the situation for a reversing wind profile. The wind at the surface is in the opposite direction to the motion aloft. Therefore shear

exists in the vertical wind profile. The precipitation particles will follow a curved trajectory from the source to the gauge. The source will be ***overhead*** rather than ***upwind*** of the gauge site.

The time taken for the precipitation particles to fall from the height of the radar sample volume to the surface (the *lag*) is a function of (a) the fall speed of the particles and (b) the height of the sample volume above the surface.

Note that in Figures 1 and 2 the elevation angle of the radar beam geometry is grossly exaggerated for clarity. In practice the beam angle used is around 0.5 degrees and the beam geometry overhead the gauge may for all practical purposes be considered horizontal.

3.3 The relationship between radar reflectivity Z and extinction coefficient E

Logic dictates that, in precipitation, as Z increases so does E. This is so because increasing the number or size of the particles leads to an increase in power returned to the radar as well as an increase in the spatial rate of light extinction. Hence the Z-E curve should be monotonically increasing.

This turns out to be true in practice. The exact relationship varies depending on the characteristics of the precipitation during a given event, but the essential nature of the relationship does not change.

Figure 3 shows the scatter-plot for all of the Z-E data for EWR for the period 2002/01/31 to 2002/04/30.

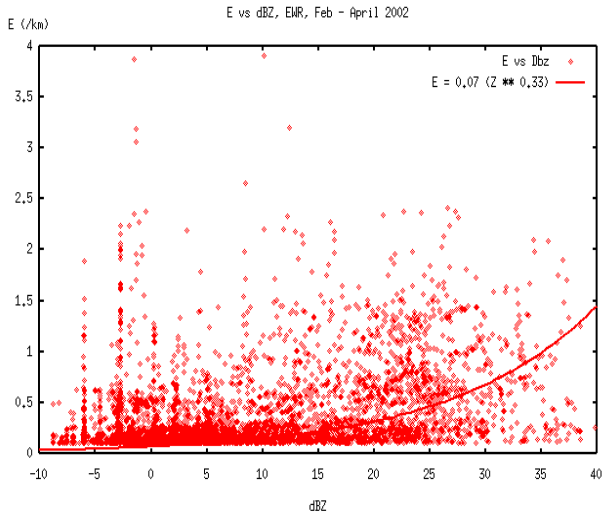

Figure 3: DBZ-E scatter plot for Z-E data for EWR

Muench and Brown (1977), in a study for the US Air Force, concluded that the relationship would have the form:

$$E = a\,Z^{b} \qquad (4)$$

The data used in their study yielded values of 0.091 for ‘a’ and 0.41 for ‘b’.

A fit of the Z-E relationship to this data yields:

$$E = 0.07\,Z^{0.33} \qquad (5)$$

Inspection of the data in Figure 3 shows that for low Z values the function asymptotes to a small positive value for E, in this case 0.07. It seems reasonable to suggest that this value represents the 'clear air' E value for the ASOS visibility instrument. This observation will be used when computing the Z-E calibration – see section 4.6.

The Muench and Brown study only included data with E values above 0.5 and dBZ values above 30. To more closely match that data set, Figure 4 shows all of the LGA, JFK and EWR data combined but truncated to exclude E values below 0.5 and dBZ values below 10. In this case the fit is:

$$E = 0.07\,Z^{0.39} \qquad (6)$$

which closely agrees with the result published by Muench and Brown.

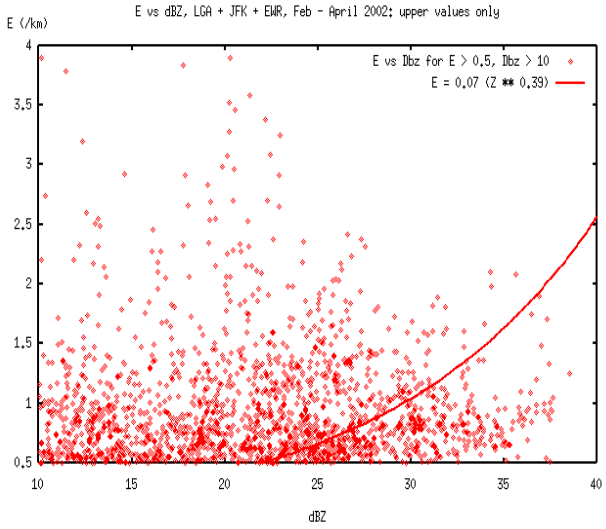

Figure 4: DBZ-E scatter plot for LGA, JFK and EWR, with E > 0.5 and dBZ > 10

The scatter in these plots is high and it is difficult to assess whether the form of the function is correct.

However, consider Figures 5 and 6, which show the Z-E data plotted for LGA and JFK respectively for a 2-hour period on 2002/03/18.

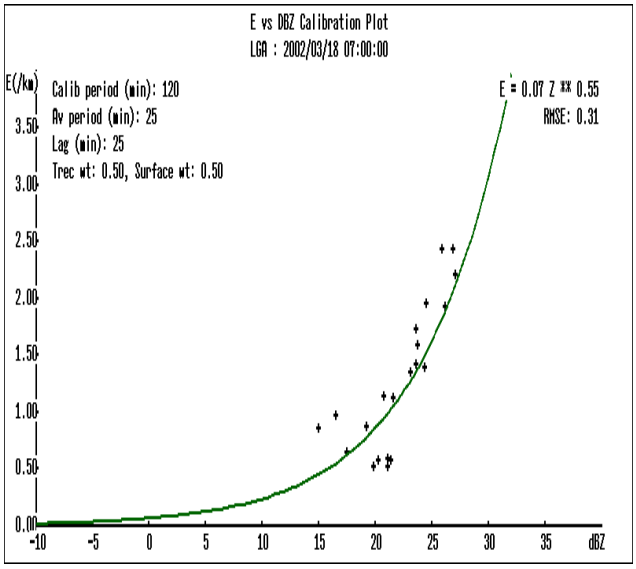

Figure 5: calibration plot for LGA 2002/03/18 05:00Z – 07:00Z

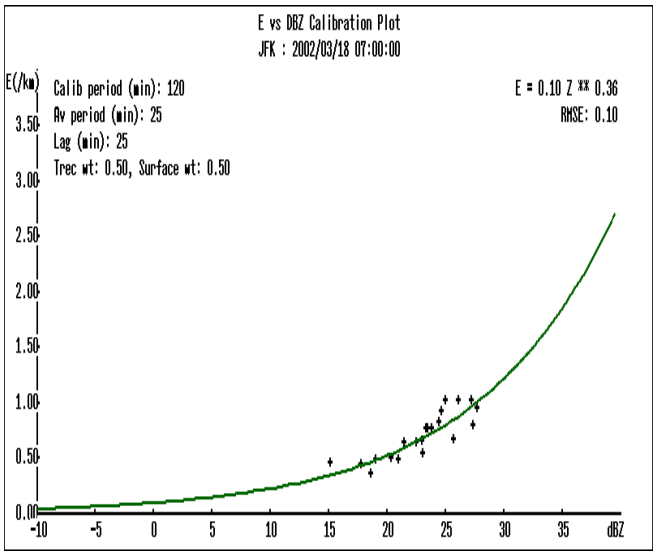

Figure 6: calibration plot for JFK 2002/03/18 05:00Z – 07:00Z

Suitable time-averaging (25 min) and lag (25 min) values have been applied to produce the plot - these issues will be dealt with in detail in later sections. The plots demonstrate the exponential relationship between Z and E, and also show the variability in the values of 'a' and 'b' for these two cases.

In these plots at the top right you will see the Z-E relationship as well as a value labeled 'RMSE'. This is the *Root Mean Square Error* of the estimate made for E by the Z-E function. It represents the mean error in E for the data used to fit the curve. It can be thought of as a measure of how well the Z-E function fits the measured values. We will make extensive use of the RMSE values later in this study to determine the optimum values for various aspects of the Z-E calibration.

4 The algorithms

4.1 Radar echo motion - TREC

Figure 7 shows the 0.5 degree PPI for the OKX radar at 07:07Z on 2002/03/18. A band of snow is moving across the New York area from west to east.

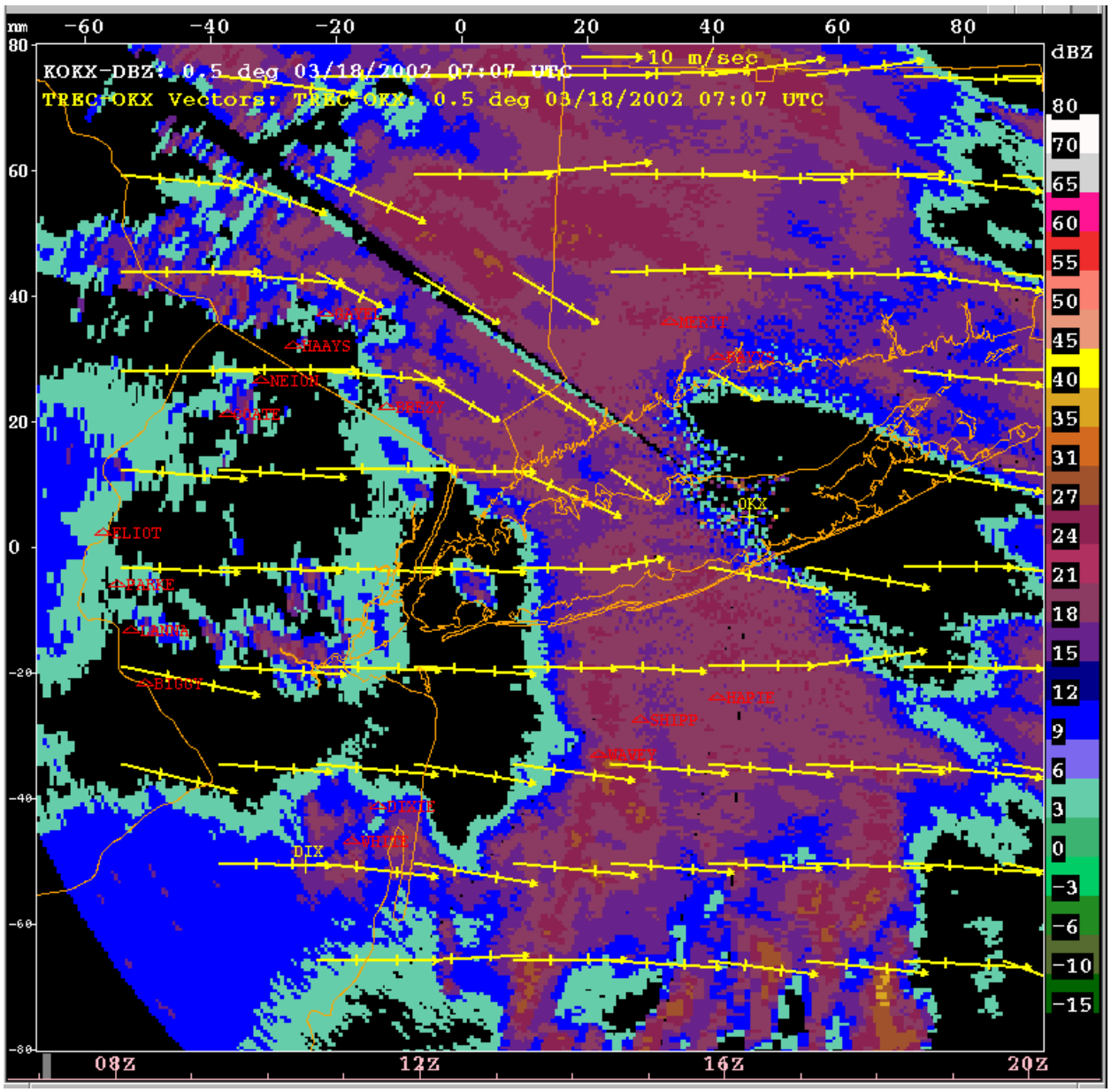

Figure 7: 0.5-degree PPI for OKX radar at 07:07Z on 2002/03/18, showing TREC motion vectors

Also shown on the figure are vectors indicating the motion of the radar echoes. These are 30-minute vectors, i.e. they indicate the distance the echo is expected to move over a 30-minute period. The tick marks on the vectors show the 10-minute motion.

The reflectivity motion is computed using the Tracking Radar Echoes by Correlation (TREC) algorithm (Rinehart and Garvey 1978, Tuttle and Foote 1990). TREC looks for motion by recognizing 2-D patterns in the reflectivity data and computing how far those patterns move with time. It also considers radial velocity and attempts to reconcile the velocity signal with the motion obtained from the reflectivity.

TREC produces a grid of U (E-W) and V (N-S) velocity components for the motion of the radar echoes.

4.2 Time series plot

Before we go further we need to introduce an example of the time series plot. We will refer back to this plot as we explain aspects of the calibration and forecasting algorithms.

Figure 8 shows the time history of radar and visibility data for LGA for 16:28Z on 2002/03/18. This figure contains much detailed information. Therefore we will explain it in detail before moving on.

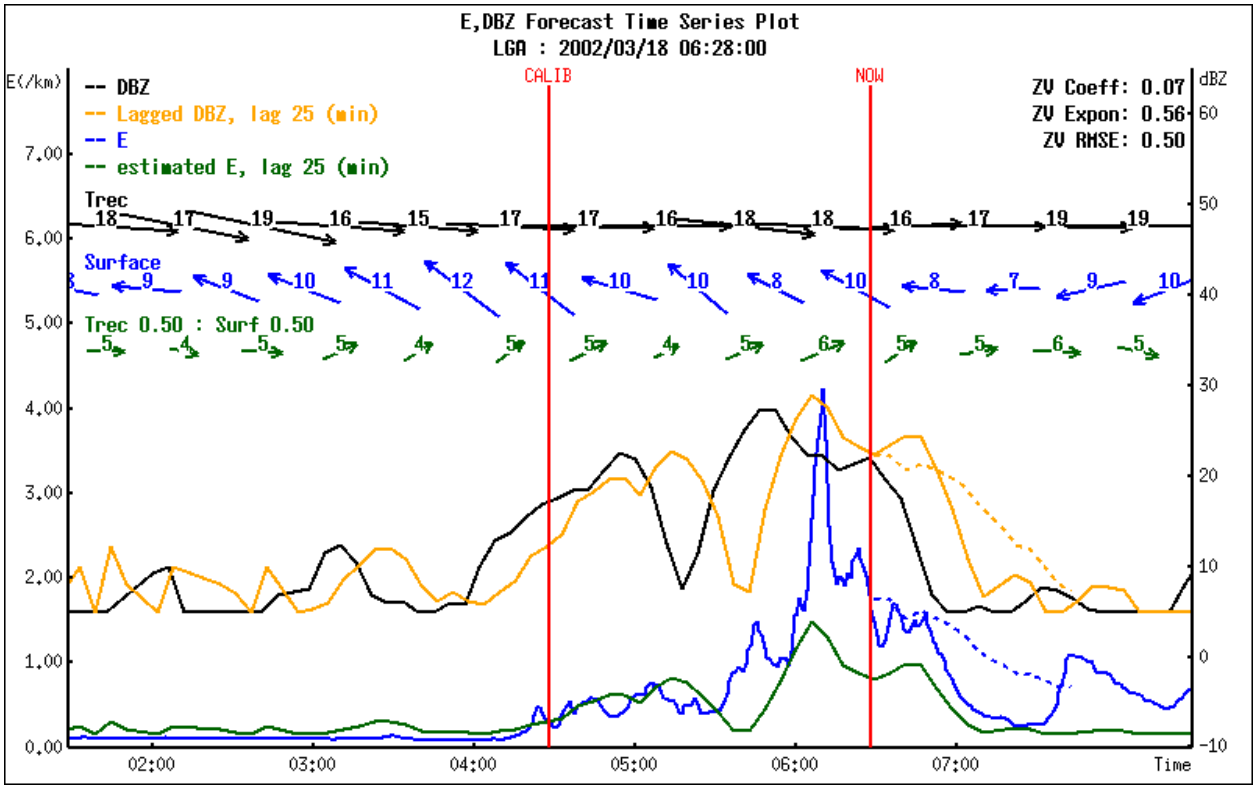

Figure 8: time series plot for LGA at 2002/03/18 06:26Z

The time axis (in UCT) is along the bottom, with the E axis on the left and the dBZ axis on the right.

The vertical red line marked 'NOW' marks the reference time for the plot. History is to the left of the line and forecasts (or 'future') to the right. In real-time operations only the forecast data would occur to the right of the NOW line. Since this is an analysis we also show what actually occurred, hence the data to the right of NOW. This can be thought of as 'truth' data.

The vertical red line marker 'CALIB' marks the start of the calibration period. The Z-E calibration is performed for data between CALIB and NOW.

The solid black line traces the dBZ ***overhead*** the gauge site.

The yellow line traces the dBZ which was measured by the radar ***upwind*** of the gauge and which theoretically has followed the particle trajectory to arrive at the gauge. It is computed by looking both upwind and back in time. Details on this procedure will be presented later.

The dotted yellow line is the reflectivity forecast – i.e., it represents the dBZ values which correspond to forecast precipitation at the gauge.

The dark blue line traces E as measured by the gauge.

The dotted blue line is the forecast for E.

The green line represents the estimated E at the gauge. It is computed by applying a Z-E calibration to the dBZ data in the yellow line.

The black vectors are the mean TREC motion vectors for a region *overhead* the gauge.

The dark blue vectors represent the measured wind at the ASOS site. In this example the surface wind opposes the TREC vectors, a situation similar to that depicted in Figure 2.

The green vectors represent the 'weighted mean motion' for the particle trajectory. They are computed as the weighted mean of the TREC and surface motion vectors. In this case the weights were set to 50/50.

The labels at the top right show the coefficient 'a' and exponent 'b' of the Z-E calibration function.

4.3 Calibration plot

Refer back to Figure 5. This is an example of a calibration plot, showing the data which is used to compute the Z-E calibration parameters. This example is for LGA at 07:00Z on 2002/03/18.

The E axis is on the left and the dBZ axis along the bottom. The data points shown plotted are those used to compute the calibration, i.e. they lie between the CALIB and NOW lines in the time series plot. The line shown is the best fit of the Z-E exponential function to the data.

The labels on the top left are as follows:

- **Calib period**: the calibration data is selected from the time period from the reference time back into the past by this number of minutes.

- **Av period**: the averaging period in minutes. If greater than 0, this indicates that the data has been smoothed through time averaging, using this number of minutes of data. It turns out that the averaging period has little effect on the computed calibration, however it is useful for helping to visualize the physics of the processes by smoothing out the noise. In Figure 5 an averaging value of 25 min was chosen.

- **Lag**: the lag time in minutes for the particle trajectory. This is the same lag as in the yellow line on the time-series plot.

- **Trec wt, Surface wt**: the weight applied to the TREC motion vectors vs. the surface motion vectors to compute the mean motion for the particle trajectory.

The Z-E coefficient ‘a’ and exponent ‘b’ are shown at the top right, along with the RMSE (root mean squared error) for the fit.

4.4 Radar-to-gauge time lag

Refer to Figure 8 and compare the black trace (dBZ *overhead* the gauge) with the blue trace (measured E). They appear well correlated but with a shift in time. Now consider the yellow line, which is the ***lagged*** reflectivity determined by looking ***upwind*** along the TREC vectors to find the reflectivity source aloft which theoretically resulted in the measured precipitation at the surface. The lag was set to 25 minutes because it minimizes the RMSE – see below.

There is an alternative way to visualize this data. Refer to Figures 9, 10, 11 and 12. These show the calibration plots for this case, using data from 05:00Z to 07:00Z, and lag times of 0, 10, 20 and 25 minutes respectively.

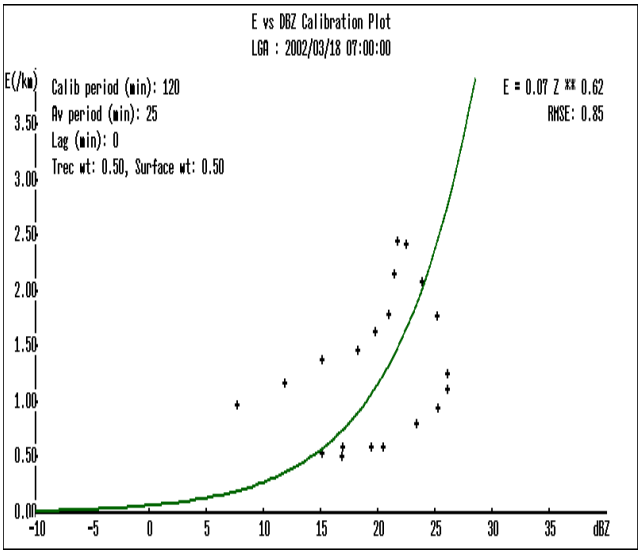

Figure 9: LGA calibration plot with lag of 0 min, showing marked hysteresis

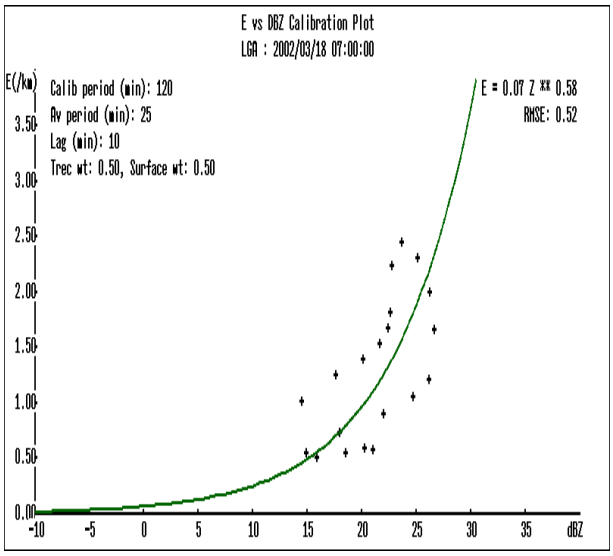

Figure 10: LGA calibration plot with lag of 10 minutes, showing moderate hysteresis

Figure 9 shows the calibration plot for this case, but with a lag of 0. Notice the apparent 'hysteresis' loop in the data. The data points early in the event, as the reflectivity starts to increase, lie below the fitted line. This occurs because the unlagged reflectivity is 'leading' the measurement of E. Later in the event, as the reflectivity starts to decrease the data points lie above the line. Also notice the RMSE value of 0.85.

Figure 10, for a lag of 10 minutes, shows a more moderate hysteresis loop and an RMSE value of 0.52. The lower RMSE reflects the fact that the fit is better than for a lag of 0.

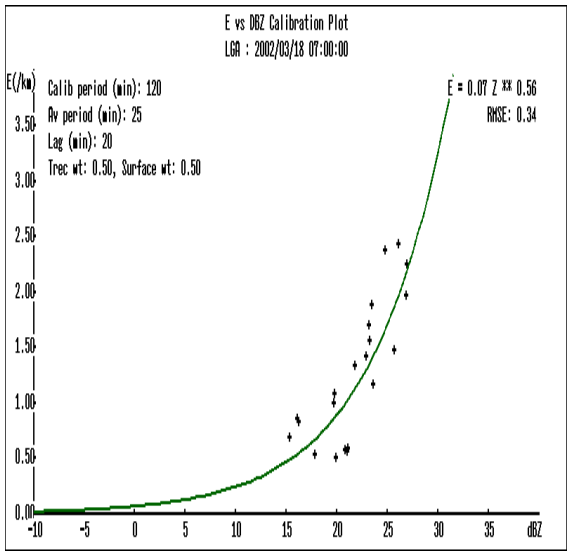

Figure 11: LGA calibration plot with lag of 20 minutes, showing reduced hysteresis

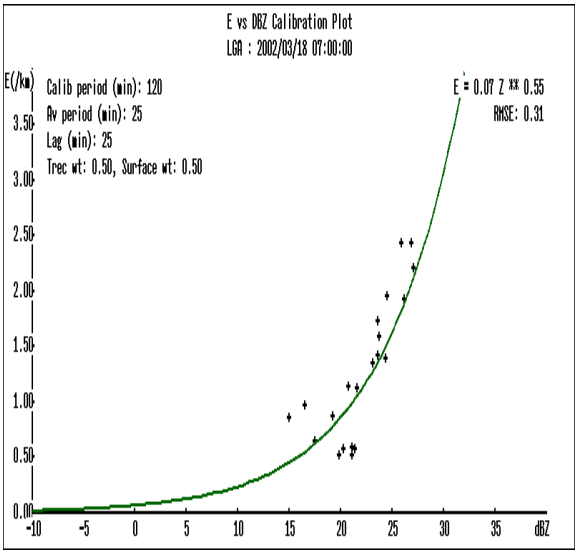

Figure 12: LGA calibration plot with lag of 25 minutes, showing minimal hysteresis

Figure 11 shows the calibration plot using a lag of 20 minutes and exhibits markedly reduced hysteresis with an RMSE value of 0.34. In Figure 12, for a 25 minute lag, the hysteresis has largely disappeared and the RMSE is 0.31.

This demonstrates that we can estimate the optimum lag by minimizing RMSE. Table 2

shows the RMSE values for lags from 0 to 40 minutes. In all cases the averaging period was 25 minutes.

Lag (Minutes)	RMSE
0	0.85
5	0.67
10	0.52
15	0.42
20	0.34
25	0.31
30	0.31
35	0.39
40	0.48

Table 2: RMSE vs. lag for LGA event at 07Z on 2002/03/18

From Table 2 it is clear that the RMSE varies smoothly with lag, reaching a well-defined minimum of 0.31 at a lag of between 25 and 30 minutes. This analysis presents a useful method for both considering the physics of what is happening and for determining the actual lag. It seems reasonable to suggest that, at least for well-defined cases such as this one, the lag can be determined by minimizing the RMSE.

By studying a number of cases at a site it should be possible to determine (a) what the optimum lag is and (b) whether this lag varies significantly from one case to another. It may even be possible to automate this procedure so that a forecasting system could 'tune' itself by finding the optimum lag. However, this hypothesis would need testing on a number of cases before it could be claimed that it would work reliably in practice.

4.5 Particle trajectory

Refer back to Figures 1 and 2, showing the theoretical trajectories of the precipitation particles falling from radar height down to the gauge location. Then consider the actual vectors plotted on Figure 8. These indicate that the TREC motion (black vectors) and surface wind (blue vectors) are opposed to each other in direction, suggesting a profile similar to that in Figure 2.

As stated previously, the particle trajectory from radar sample volume to gauge is dependent on the vertical wind profile from the surface to radar beam height. In an ideal situation a wind profiler would provide that information. However, these instruments are not yet widely deployed. Therefore we need to infer the profile from the information we have at each extreme, the TREC vectors at radar beam height and the ASOS wind vector at the surface.

We postulate that we can compute the mean trajectory motion vector as a weighted mean of the TREC and surface vectors.

Figures 13, 14 and 15 show the calibration plots for LGA, varying the weights given to the TREC motion vectors and the surface motion vectors. Figure 13 shows one extreme, with TREC weighted 100% weight and Figure 14 represents the other extreme with TREC weighted 0%. Figure 15 is in between with TREC at 40%. Once again the RMSE values for the fit reflect how well the calibration curve represents the data. Inspection of the data also reveals hysteresis-type behavior, though less easily understood than that in Figures 9 through 12. What is clear from inspection is that the data in Figure 15 makes physical sense while that in the other two plots probably does not. We can conclude that the wind profile represented by the weights in Figure 15 reflects the true profile more accurately than either Figure 13 or 14.

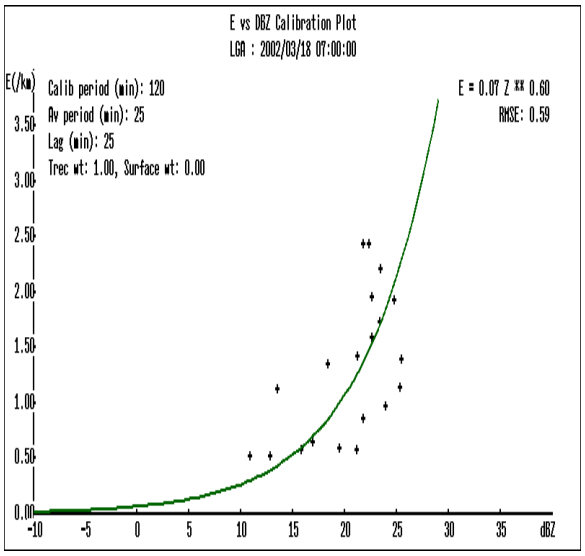

Figure 13: LGA calibration plot, TREC vector wt. 100%, surface vector wt. 0%

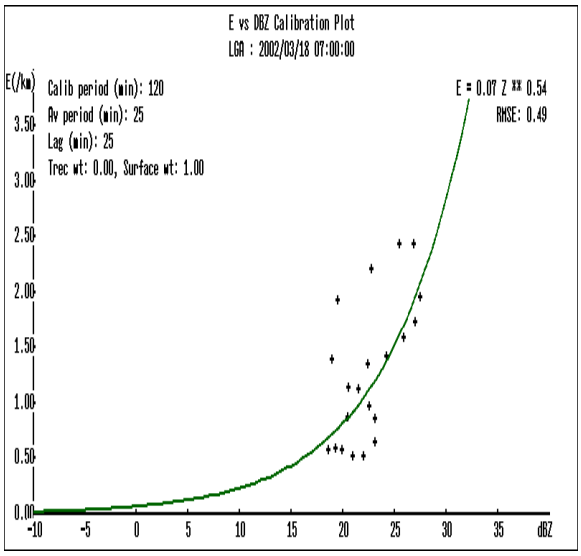

Figure 14: LGA calibration plot, TREC vector wt. 0%, surface vector wt. 100%

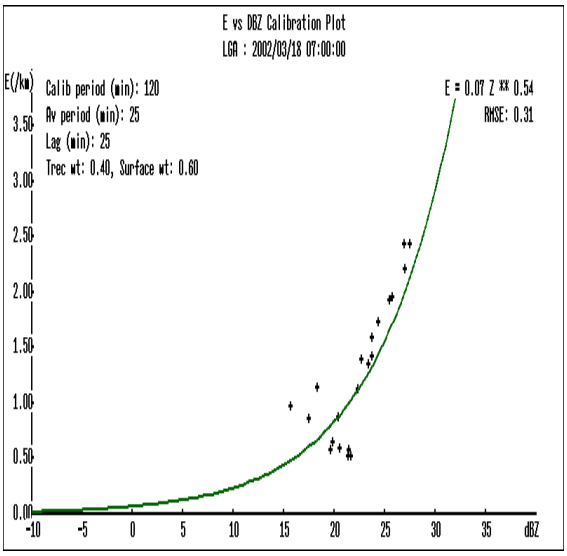

Figure 15: LGA calibration plot, TREC vector wt. 40%, surface vector wt. 60%

Table 3 shows the RMSE analysis in more detail, varying the weights by 10% each time.

TREC weight	Surface weight	RMSE
100%	0%	0.59
90%	10%	0.56
80%	20%	0.53
70%	30%	0.43
60%	40%	0.34
50%	50%	0.31
40%	60%	0.31
30%	70%	0.34
20%	80%	0.41
10%	90%	0.45
0%	100%	0.49

Table 3: RMSE values for Z-E calibration for various TREC/Surface motion weights, LGA, 07Z 2002/03/18

Once again, the RMSE varies smoothly, indicating that this is a deterministic method for finding the optimum. In this case the optimum

lies somewhere between 50/50 and 40/60 with an RMSE of 0.31.

4.6 E vs. Z calibration

Sections 4.1 to 4.5 above lay the groundwork for performing the Z-E calibration. It is essential to determine the TREC motion, lag and wind profile weights accurately before proceeding with the calibration.

As stated in section 3.3, the Z-E relationship takes the form:

$$E = a Z^{b} \quad (7)$$

This is a function with 2 unknowns, ‘a’ and ‘b’. Finding a good fit to a function with 2 degrees of freedom is not possible with data sets which are either small or noisy.

Instead, we first determine ‘a’ using logical arguments and then compute ‘b’ statistically. This yields a more stable and robust result.

4.6.1 Coefficient 'a'

As stated in section 3.3, the coefficient 'a' has a physical basis. Since it is the asymptote of the Z-E function for low values of Z, it corresponds to the 'clear air' measurement of E. In other words, it is the E value measured by the gauge when the visibility is effectively unlimited.

One option would be to use the lowest E value recorded in the recent past, say the previous 30 days. However, this is susceptible to outliers and noise in the system. As a more robust measure than the minimum, we decided to use the 0.25% quartile of the E values observed over the past 30 days. The 0.25 % quantile is the E value which is exceeded by 99.75% of the data in the chosen sample. In other words, it is very close to the minimum, but is not actually the minimum.

4.6.2 Exponent 'b'.

Once the coefficient ‘a’ has been determined, the problem reduces to a statistical fit with one degree of freedom. For example, suppose that we determine that the value of ‘a’ is 0.07. Then the equation to fit from the data is:

$$E = 0.07 Z^{b} \quad (8)$$

Taking natural logs on both sides yields:

$$\ln(E) = \ln(0.07) + b \ln(Z) \quad (9)$$

This is a linear fit problem, which is trivial to solve. It is also robust and insensitive to noise. We can demonstrate this by solving for ‘b’ on data sets which have been smoothed to varying degrees.

Table 4 shows the b values determined for the LGA case at 07Z on 2002/03/18, along with the RMSE values, for various degrees of temporal smoothing.

Averaging period (min)	Exponent ‘b’	RMSE
0	0.58	0.52
5	0.58	0.52
10	0.58	0.51
15	0.57	0.41
20	0.57	0.40
25	0.55	0.31
30	0.55	0.30
35	0.54	0.27
40	0.54	0.25

Table 4: Exponent 'b' and RMSE values for LGA data from 05Z to 07Z on 2002/03/18 for varying averaging periods

The RMSE values drop steadily with smoothing as would be expected. The value of ‘b’ is not significantly affected. It probably makes sense to use a moderate degree of smoothing for the calibration, say 15 minutes.

4.7 Making the forecast

The sections above present a method for calibrating the radar reflectivity Z with gauge-measured E values. The purpose is to convert a reflectivity forecast into a forecast of E values. We have also shown how to find the optimal values for radar-to-gauge time lag and the mean motion vector for the particle trajectory, both of which affect the forecast.

First we need to make a reflectivity forecast at the surface. This is done by looking upwind and

back in time for the source region of reflectivity at the radar beam height which will produce precipitation at the ground in the future.

There are two components of the search upwind: (a) *particle trajectory* and (b) *echo advection at radar height*. The problem can be framed in the following way: suppose that the lead time is the same as the lag. Then the source area for particles reaching the ground is the start of the particle trajectory, i.e. the point at which it was detected by radar. However, if the lead time is longer that the lag, the radar echo must first advect into position before the particles begin to fall.

To summarise:

(a) ***particle trajectory***: forecast lead time <= lag time. Search upwind using the mean motion vector.

(b) ***echo advection****:* forecast lead time > lag time. First search upwind using the mean motion vector, then search further upwind using the TREC vector.

This is best illustrated with an example. See table 5.

Forecast lead time	Radar image time	Time upwind for trajectory	Time upwind for advection
0 min	25 min ago	25 min	0 min
5 min	20 min ago	25 min	0 min
10 min	15 min ago	25 min	0 min
15 min	10 min ago	25 min	0 min
20 min	5 min ago	25 min	0 min
25 min	now	25 min	0 min
30 min	now	25 min	5 min
35 min	now	25 min	10 min
40 min	now	25 min	15 min
45 min	now	25 min	20 min
etc ...			

Table 5: finding the source reflectivity for various lead times, given a lag of 25 minutes

Suppose we have the situation found at LGA in the case considered above, with a time lag of 25 minutes. Then the source reflectivity would be searched using the time rules in Table 5.

Once the reflectivity forecast has been computed, we apply the Z-E relationship to the dBZ values to compute the forecast for E.

The dBZ forecast is shown in Figure 8 as the dotted yellow line, and the E forecast as the dotted blue line.

5 Conclusions

This study demonstrates the feasibility of making short-term visibility forecasts based on NEXRAD radar data and ASOS ground measurements.

Specifically we can conclude the following:

- There exists a plausible functional relationship between E and Z which has a physical basis.
- It is possible to correlate reflectivity values measured by radar with surface visibility measurements from ASOS by taking into account the following factors:
  a) the advection of the radar echoes
  b) the time lag from radar to gauge
  c) the vertical wind profile from the radar measurement height down to the surface.
- It is possible to determine the values for echo advection, time lag and vertical wind profile in a deterministic manner.
- Using the above parameters, it is possible to make a physically-based forecast of E from the radar and ASOS data.

6 Future improvements

This study considered the feasibility of making a short-term visibility forecast using radar and ASOS data. The results are promising. However, the following enhancements could improve the accuracy of the forecasts.

6.1 Enhancements to TREC

Accurate TREC vectors are vital for producing good forecasts. TREC has two known problems in snow events:

- The NEXRAD radar processor uses a notch filter in the zero-velocity region for clutter removal. This leads to a gap in the data where the radial velocity is close to 0, even if there is no clutter. This gap always occurs in stratiform situations, with the location of the gap depending on the wind direction.
- Consistent beam blockage confuses TREC. Refer back to OKX radar data in Figure 7. There is a narrow sector of missing data in the NW quadrant. This is always present for OKX at the 0.5 degree elevation. The missing data is caused by beam blockage from an obstruction on the ground, probably a tall structure. You will notice that the TREC vectors tend to align themselves with the missing data area. This occurs because TREC is depends on pattern recognition and the movement of those patterns. Since the missing sector itself does not move, TREC tends not to compute motion across it. Therefore the vectors tend to be parallel to the missing zone even though the real motion is across it.

We suggest spending some effort on improving TREC to handle these types of problem.

6.2 Discrimination between rain and snow

It is possible that the reliability of the forecast could be improved by discriminating between rain and snow events. The ASOS LEDWI instrument may prove useful in this regard.

ACKNOWLEDGEMENTS

NCAR is sponsored by the National Science Foundation. This research is in response to requirements and funding by the Federal Aviation Administration (FAA). The views expressed are those of the authors and do not necessarily represent the official policy of the FAA.

REFERENCES

Huschke, R., Ed., 1959: Glossary of Meteorology. Amer. Meteor. Soc., 638 pp.

Nadolski, V. L. and M. D. Gifford, 1995: An Overview of ASOS Algorithms. 6th Conference on Aviation Weather Systems, AMS.

Muench, H. S. and H. A. Brown, 1977: Measurement of Visibility and Radar Reflectivity During Snowstorms in the AFGL Mesonet. Project 8628, Met Division, Air Force Geophysics Laboratory, Hanscom AFB, Massachusetts. AGFL-TR-77-0148.

Rinehart, R.E. and E.T Garvey, 1978: Three-dimensional storm motion detection by conventional weather radar. Nature, 273, 287-289.

Tuttle, J. D. and G.B Foote, 1990: Determination of the boundary layer airflow from a single Doppler radar. J. Atmos. Oceanic tmicrophysical retrieval from Doppler radar observations using a cloud model and its adjoint. Part I: Model development and simulated data experiments. J. Atmos Sci. **54**, 1642-1661.

Weygandt S. S., A Shapiro, K.K. Droegemeier, 2002: Retrieval of Model Initial Fields from Single-Doppler Observations of a Supercell Thunderstorm. Part I: Single-Doppler Velocity Retrieval. Mon. Wea. Rev. **130**, 433-453.